N–B **1** compound. At −10 °C there is a complete disappearance of the peaks assigned to $Me_2PNMe_2{\cdot}BH_3$ and Me_2PNMe_2, and only the peaks due to **2** and **3** are observed. If the reaction mixture is maintained at −60 °C for 24 h, $Me_2PNMe_2{\cdot}2BH_3$ is obtained in quantitative yields. The ^{11}B NMR spectrum now contains only two resonances of equal intensity associated with B–N and B–P coordination in **3** (See Table I). The NMR assignments for **2** have been confirmed by the synthesis of **2** and a comparison with the literature values.[10]

The bis(borane) adduct has been isolated by carrying out the reaction at −10 °C in a THF/toluene solvent mixture. Trap-to-trap fractionation at −10 °C gives a white solid, $Me_2PNMe_2{\cdot}2BH_3$, in 85% yield. Satisfactory elemental analyses were obtained. This compound is quite stable thermally as indicated by its melting point (117 °C) and mass spectral data. The presence of a molecular ion (*m/e* 133) and the peaks corresponding to the fragmentation of the parent aminophosphine are noted in the mass spectrum.

Further work is in progress to determine the generality of such reactions and to study the steric and electronic factors that influence the relative basicities of these donor atoms.

Acknowledgment. The support of this research by the University College Committee on Faculty Research Grants at the University of Alabama at Birmingham is gratefully acknowledged.

Department of Chemistry
University of Alabama at Birmingham
Birmingham, Alabama 35294

Ravindra K. Kanjolia
Charles L. Watkins*
Larry K. Krannich

Received June 25, 1986

Articles

Contribution from the Chemical Thermodynamics Laboratory, Faculty of Science, Osaka University, Toyonaka, Osaka 560, Japan, and School of Chemical Sciences, University of Illinois, Urbana, Illinois 61801

Heat Capacity and Phase Transitions of the Mixed-Valence Compound $[Fe_3O(O_2CCH_3)_6(3\text{-Me-py})_3]{\cdot}3\text{-Me-py}$[1]

Michio Sorai,*[2] Yutaka Shiomi,[2] David N. Hendrickson,*[3] Seung M. Oh,[3] and Takeshi Kambara[3,4]

Received June 26, 1986

The heat capacity under constant pressure, C_p, of oxo-centered mixed-valence $[Fe_3O(O_2CCH_3)_6(3\text{-Me-py})_3]{\cdot}3\text{-Me-py}$ has been measured with an adiabatic calorimeter between 12 and 350 K, where 3-Me-py is 3-methylpyridine. Four phase transitions were found to occur at 181, 263.5, 271.5, and 282.5 K. The cumulative enthalpy and entropy changes due to these four phase transitions were calculated to be $\Delta_{trs}H = 3410 \pm 130$ J mol^{-1} and $\Delta_{trs}S = 13.71 \pm 0.65$ J K^{-1} mol^{-1}, respectively. By comparison of the present results with the ^{57}Fe Mössbauer spectroscopy and the X-ray structural work already done for this complex, it is concluded that these phase transitions involve at various temperatures intramolecular electron transfer in the mixed-valence Fe_3O complexes and the order–disorder phenomenon of the pyridine solvate molecules jumping between two energetically equivalent positions in the solid state. The contributions from these two phenomena to the transition entropy are R ln 3 and R ln 2, respectively, and the sum is 14.90 J K^{-1} mol^{-1}. This accounts well for the observed value of 13.71 ± 0.65 J K^{-1} mol^{-1}. DTA thermograms for the solid solutions of $[Fe^{III}_2Fe^{II}_{1-x}Co^{II}_xO(O_2CCH_3)_6(3\text{-Me-py})_3]{\cdot}3\text{-Me-py}$, where $x = 0$, 0.25, 0.5, 0.75, and 1.0, have been recorded between 80 and 350 K. The highest temperature phase transition found for the $x = 0.0$ compound is linearly shifted to a lower temperature with increasing x. The concentration dependence of the transition temperature, $T_C(x)$, is described by the linear equation $T_C(x)$ (K) $= 282.54 - 13.08x$. The lowest temperature phase transition at 181 K is easily undercooled. By comparison of the molar entropies of the undercooled and nonundercooled states at a common temperature (196.8395 K in the present case), it has been concluded that the undercooled phase has no residual entropy, that is, the molecules in this phase are in an ordered state at 0 K. A model for the observed phase transitions has been devised that accounts for all of the X-ray structural, spectroscopic, and heat capacity results for $[Fe_3O(O_2CCH_3)_6(3\text{-Me-py})_3]{\cdot}3\text{-Me-py}$. Below 181 K all three iron ions are inequivalent and only one vibronic state of the Fe_3O complex is populated. At 181 K the thermal energy becomes comparable to intermolecular interactions and there is a phase transition such that the potential-energy diagram of the Fe_3O complex changes. At temperatures above 181 K two vibronic states (i.e., two minima in the potential-energy diagram) are populated. Finally, in the high-temperature phase transition which culminates at 282.5 K and has two anomalies at 263.5 and 271.5 K there is an onset of motion involving the 3-Me-py solvate molecule jumping between its two lattice sites. As a result the Fe_3O complex tends to become more equilateral than it is at low temperatures and all three vibronic states of the Fe_3O complex are populated to some degree.

Introduction

A recent exciting finding is that the rate of *intra*molecular electron transfer for a mixed-valence transition-metal complex in the solid state is significantly influenced by the onset of motion of ligands, solvate molecules, and/or counterions.[5-18] In the case of oxo-centered mixed-valence $[Fe_3O(O_2CCH_3)_6(py)_3]{\cdot}py$ (py = pyridine), for example, the orientational order–disorder phenom-

(1) Contribution No. 100 from the Chemical Thermodynamics Laboratory.
(2) Osaka University.
(3) University of Illinois.
(4) On sabbatical leave from the Department of Engineering Physics, The University of Electro-Communications, Chofu, Tokyo 182, Japan.
(5) Oh, S. M.; Hendrickson, D. N.; Hassett, K. L.; Davis, R. E. *J. Am. Chem. Soc.* **1984**, *106*, 7984.
(6) Oh, S. M.; Kambara, T.; Hendrickson, D. N.; Sorai, M.; Kaji, K.; Woehler, S. E.; Wittebort, R. J. *J. Am. Chem. Soc.* **1985**, *107*, 5540.
(7) Oh, S. M.; Hendrickson, D. N.; Hassett, K. L.; Davis, R. E. *J. Am. Chem. Soc.* **1985**, *107*, 8009.
(8) Woehler, S. E.; Wittebort, R. J.; Oh, S. M.; Hendrickson, D. N.; Inniss, D.; Strouse, C. E. *J. Am. Chem. Soc.* **1986**, *108*, 2938–2946.
(9) Sorai, M.; Kaji, K.; Hendrickson, D. N.; Oh, S. M. *J. Am. Chem. Soc.* **1986**, *108*, 702–708.
(10) Details of the X-ray structure, Mössbauer, and solid-state ^2H NMR results for $[Fe_3O(O_2CCH_3)_6(py)_3]{\cdot}py$: Woehler, S. E.; Wittebort, R. J.; Oh, S. M.; Kambara, T.; Hendrickson, D. N.; Inniss, D.; Strouse, C. E. *J. Am. Chem. Soc.*, in press.

0020-1669/87/1326-0223$01.50/0

enon of the pyridine solvate molecule about a crystallographic C_3 axis is strongly correlated with intramolecular electron transfer in the Fe_3O complex.[6,9,10] In fact, the onset of the pyridine solvate rotation has been found to contribute $R \ln 3$ (R is the gas constant) to the phase transition entropy.[6,9] The onset of rotation of the pyridine solvate molecules, as well as the electronic localization–delocalization transformation, in $[Fe_3O(O_2CCH_3)_6(py)_3]\cdot py$ occurs as a phase transition because of appreciable *inter*molecular interactions in the solid state.[18] The Fe_3O complexes are assembled in stacks with each pyridine solvate molecule sandwiched between two Fe_3O complexes. The onset of rotation of the solvate molecules changes the ground-state potential-energy diagram for each Fe_3O complex, and this changes its *intra*molecular electron-transfer characteristics.

For comprehensive understanding of a phenomenon such as order–disorder phase transitions, information on both structural and energetic types is of complementary importance. From variable-temperature heat-capacity measurements it is possible to derive fundamental thermodynamic quantities such as enthalpy, entropy, and free energy. Calorimetric study of phase transitions often occurring in the solid state provides us with definitive evidence of what has happened in such catastrophic phenomena. This can be achieved by the inherent characteristics of thermodynamics, where for thermal excitations there exist no selection rules that are intrinsic features of various spectroscopies.

In a recent paper,[11] the electron-transfer characteristics of the series $[Fe_3O(O_2CCH_3)_6(3\text{-Me-py})_3]\cdot S$, where S is a solvate molecule such as 3-Me-py (3-methylpyridine), toluene, benzene, or CH_3CN, have been characterized by a combination of single-crystal X-ray structural, ^{57}Fe Mössbauer, and solid-state ^2H NMR techniques. It was found that the CH_3CN solvate complex does *not* exhibit an increasing rate of electron transfer with increasing temperature, whereas the other three complexes do experience rapid (rate $> \sim 10^7\ s^{-1}$) electron transfer at room temperature. Variable-temperature solid-state ^2H NMR data clearly indicated that in the case of the S = toluene complex the onset of motion involving the toluene solvate molecules jumping between two lattice positions (i.e., dynamic disorder) led to the temperature dependence observed in the rate of intramolecular electron transfer for the Fe_3O complexes.

In this paper data from the measurement of the heat capacity under constant pressure, C_p, are presented for $[Fe_3O(O_2CCH_3)_6(3\text{-Me-py})_3]\cdot 3\text{-Me-py}$ in the range 12–350 K. The changes in entropy associated with two phase transitions that are observed are analyzed in terms of various phenomena indicated to be present by structural and spectroscopic techniques. For additional insight, DTA data are also presented for the toluene solvate complex, as well as for solid solutions of the composition $[Fe^{III}_2Fe^{II}_{1-x}Co^{II}_xO(O_2CCH_3)_6(3\text{-Me-py})_3]\cdot 3\text{-Me-py}$, where x = 0.25, 0.50, 0.75, and 1.0.

Experimental Section

Compound Preparation. 3-Methylpyridine (3-Me-py) was dried by refluxing with BaO and then fractionally distilled under vacuum. Acetonitrile was dried over P_2O_5 and distilled under an argon atmosphere. All elemental analyses were performed in the Microanalytical Laboratory of the School of Chemical Sciences, University of Illinois. Due to the sensitivity to air and water of the compounds in solution and to a lesser degree in the solid state, reactions were carried out under an argon atmosphere in either Schlenk vessels or in an inert-atmosphere glovebox (Vacuum Atmospheres Corp.).

$[Fe_3O(O_2CCH_3)_6(H_2O)_3]$. This mixed-valence compound was prepared by a previously reported method.[19] A 20-g (0.1-mol) sample of $FeCl_2\cdot 4H_2O$, 20 g (0.24 mol) of sodium acetate, and 60 g (1 mol) of glacial acetic acid were dissolved in 100 mL of water. The reaction mixture was heated at 70–80 °C under reflux for 2 h, while a constant stream of air was bubbled. The mixture was cooled to room temperature, and the dark brown precipitate was filtered, washed with ethanol and ethyl ether, and then dried under vacuum. The yield was 10.4 g (52.7%).

$[Fe_3O(O_2CCH_3)_6(3\text{-Me-py})_3]\cdot 3\text{-Me-py}$. Samples of this compound were prepared by the method given by Lupu and Ripan[20] for the preparation of $[Fe_3O(O_2CCH_3)_6(py)_3]\cdot py$. A 5-g (8.4-mmol) amount of $[Fe_3O(O_2CCH_3)_6(H_2O)_3]$ was dissolved in 30 mL of 3-methylpyridine under an argon atmosphere. The reaction mixture was stirred for 1 h at 50–60 °C and then slowly evaporated for 3 days. The black crystalline product was filtered off and dried under vacuum. Anal. Calcd for $C_{36}Fe_3H_{46}N_4O_{13}$: C, 47.50; Fe, 18.41; H, 5.09; N, 6.15. Found: C, 47.33; Fe, 18.35; H, 5.03; N, 6.02.

$[Fe_2CoO(O_2CCH_3)_6(H_2O)_3]$. Samples of this compound were prepared by a modified method of Weinland and Holtmeier.[21] A 0.02-mol quantity of $Fe(NO_3)_3\cdot 9H_2O$, 0.01 mol of $Co(NO_3)_2\cdot 6H_2O$, and 0.2 mol of anhydrous sodium acetate were dissolved in 60 mL of distilled water and stirred for 1 day at room temperature. The resulting precipitate was filtered, washed with 50 mL of ethyl ether, and dried under vacuum for 3–4 days. The yield was 60–80%.

$[Fe_2CoO(O_2CCH_3)_6(3\text{-Me-py})_3]\cdot 3\text{-Me-py}$. A 4-g (6.7-mmol) amount of $[Fe_2CoO(O_2CCH_3)_6(H_2O)_3]$ was dissolved in 50 mL of 3-methylpyridine at 50–60 °C, and some impurities were filtered off. The filtrate was stored for 4 days in a glovebox. The resulting black crystalline product was filtered and dried. The yield was 4.21 g (73.3%). Anal. Calcd for $C_{36}Fe_2CoH_{46}N_4O_{13}$: C, 47.21; Fe, 12.34; Co, 6.31; H, 5.10; N, 6.18. Found: C, 47.34; Fe, 12.23; Co, 6.45; H, 5.08; N, 6.13.

The solid solutions of composition **$Fe^{III}_2Fe^{II}_{1-x}Co^{II}_xO(O_2CCH_3)_6(3\text{-Me-py})_3]\cdot 3\text{-Me-py}$**, where x = 0.25, 0.50, and 0.75, were prepared by dissolving the appropriate amount of $[Fe_3O(O_2CCH_3)_6(H_2O)_3]$ and $[Fe_2CoO(O_2CCH_3)_6(H_2O)_3]$ in 3-methylpyridine in a glovebox. Slow evaporation gave black crystalline precipitates that gave good analytical data.

Differential Thermal Analysis (DTA). The thermal properties of the compounds $Fe^{III}_2Fe^{II}_{1-x}Co^{II}_xO(O_2CCH_3)_6(3\text{-Me-py})_3]\cdot 3\text{-Me-py}$ (x = 0.0, 0.25, 0.5, 0.75, 1.0) were preliminarily examined by a home-built DTA apparatus in the temperature range from 80 to 350 K. As this apparatus was not equipped with a regulator controlling the cooling rate, the probe was cooled rapidly at the initial stage of cooling: a typical average rate was −5.5 K min^{-1} in the range 300–200 K, −1.7 K min^{-1} at 200–170 K, and −1.0 K min^{-1} at 170–80 K. In contrast, the heating was carried out at a constant rate of ~2.5 K min^{-1}.

Heat Capacity Measurements. Heat capacities were measured with an adiabatic calorimeter[22] between 12 and 350 K. A calorimeter cell made of gold and platinum[23] was filled with 15.0964 g (or 0.016 583 6 mol) of polycrystalline $[Fe_3O(OAc)_6(3\text{-Me-py})_3]\cdot 3\text{-Me-py}$ with buoyancy correction assuming a density of 1.4 g cm^{-3}. A small amount of helium gas was sealed in the cell to aid the heat transfer.

Results and Discussion

The cooling and heating DTA thermograms for $[Fe_3O(O_2CCH_3)_6(3\text{-Me-py})_3]\cdot 3\text{-Me-py}$ show a peak centered at an identical temperature, 282.5 K. The shape of this peak is characterized by a long tail at the low-temperature side running down to ~245 K. With only these DTA thermograms in hand it was thought that the present mixed-valence complex gives rise only to a single phase transition at T_C = 282.5 K.

The first series of calorimetric measurements was carried out to elucidate the gross aspects of this phase transition. The

(11) Details of the structural and spectroscopic results on $[Fe_3O(O_2CCH_3)_6(3\text{-Me-py})_3]\cdot S$, where S = CH_3CN, toluene, and 3-Me-py: Oh, S. M.; Wilson, S. R.; Hendrickson, D. N.; Woehler, S. E.; Wittebort, R. J.; Inniss, D.; Strouse, C. E. *J. Am. Chem. Soc.*, in press.
(12) Hendrickson, D. N.; Oh, S. M.; Dong, T.-Y.; Kambara, T.; Cohn, M. J.; Moore, M. F. *Comments Inorg. Chem.* **1985**, *4*, 329–349.
(13) Cohn, M. J.; Dong, T.-Y.; Hendrickson, D. N.; Geib, S. J.; Rheingold, A. L. *J. Chem. Soc., Chem. Commun.* **1985**, 1095.
(14) Dong, T.-Y.; Cohn, M. J.; Hendrickson, D. N.; Pierpont, C. G. *J. Am. Chem. Soc.* **1985**, *107*, 4777.
(15) Dong, T.-Y.; Hendrickson, D. N.; Iwai, K.; Cohn, M. J.; Geib, S. J.; Rheingold, A. L.; Sano, H.; motoyama, I.; Nakashima, S. *J. Am. Chem. Soc.* **1985**, *107*, 7996.
(16) Dong, T.-Y.; Hendrickson, D. N.; Pierpont, C. G.; Moore, M. F. *J. Am. Chem. Soc.* **1986**, *108*, 963–971.
(17) Dong, T.-Y.; Kambara, T.; Hendrickson, D. N., submitted for publication.
(18) Kambara, T.; Hendrickson, D. N.; Sorai, M.; Oh, S. M. *J. Chem. Phys.* **1986**, *85*, 2895–2909.
(19) Johnson, M. K.; Cannon, R. D.; Powell, D. B. *Spectrochim. Acta, Part A* **1982**, *38A*, 307.
(20) Lupu, D.; Ripan, R. *Rev. Roum. Chim.* **1971**, *16*, 43.
(21) Weinland, R. F.; Holtmeier, H. *Z. Anorg. Allg. Chem.* **1928**, *173*, 49.
(22) Yoshikawa, M.; Sorai, M.; Suga, H.; Seki, S. *J. Phys. Chem. Solids* **1983**, *44*, 311.
(23) Tsuji, K.; Sorai, M.; Suga, H.; Seki, S. *Mol. Cryst. Liq. Cryst.* **1979**, *55*, 71.

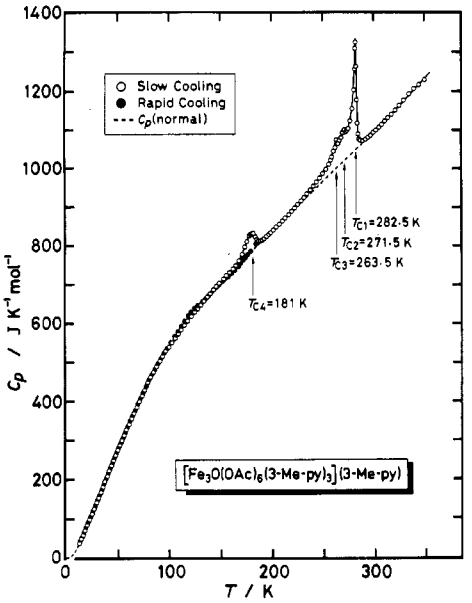

Figure 1. Molar heat capacity of $[Fe_3O(OAc)_6(3\text{-Me-py})_3]\cdot 3\text{-Me-py}$. The broken curve indicates the normal heat capacity.

specimen was slowly cooled through T_C to 268 K, and then the calorimetric measurements were started. Here, "slow cooling" means the cooling rate of −4 K h^{-1} or less. the results were evaluated in terms of C_p, the molar heat capacity at constant pressure. The experimental data are listed in Table I and plotted in Figure 1. The thermal anomaly detected by DTA was clearly observed by the heat capacity measurements as a phase transition at 282.5 K. Thermal relaxation time, the time required for thermal equilibrium in the specimen after an electric-energy input to the calorimeter cell, was shorter than 15 min even in the vicinity of T_C. This is the intrinsic time scale of the present calorimeter in this temperature region. In other words, this phase transition can attain its thermal equilibrium in a short time.

Series 2 (see Table I) corresponds to the heat capacity measurements for the specimen cooled slowly from 290 to 230 K and then cooled rapidly to 12 K, where "rapid cooling" indicates a rate of about −2 K min^{-1}. The heat capacity measurements starting from 12 K were quite normal up to ~170 K. Above this temperature, however, exothermic temperature drift due to heat evolution was observed. This fact suggested that the specimen was either in a thermodynamically nonequilibrium state or in a metastable state. We then stopped the measurement at 178 K and annealed the specimen for 18.5 h while keeping the adiabatic condition. Series 3 corresponds to the heat capacity for the specimen thus treated. Instead of the exothermic effect, an endothermic temperature drift arising from a long thermal relaxation lasted for about 1 h in this series. As shown in Figure 2, the C_p value of the first point of series 3 at T = 180.893 K jumped by ~45 J K^{-1} mol^{-1} from the extrapolated curve of series 2. The second and third points at 184.374 and 187.425 K descended, and then the remaining three points of this series recovered a normal convex form of the C_p vs. T curve. This behavior of C_p strongly suggested the existence of a phase transition around 180 K. Series 4 data were then collected to elucidate the details of this hidden phase transition. As a result of the series 4 measurements, a broad but definite peak centered at 181 K appeared. This can be regarded as a phase transition. Series 5 and 6 measurements were run to test the reproducibility of the phase transitions at 282.5 and 181 K, respectively.

The heat capacity measurements of series 7 were made to see the thermal behavior of the undercooled state below the phase transition at 181 K. To this end, the specimen was rapidly cooled from 200 to 157 K and the measurements were immediately made from 157 to 195 K without annealing. The phase transition definitely disappeared. Closely inspecting the C_p data of series 7, however, one can recognize a broad and very small hump over the range from ~170 to ~190 K. This was caused by the

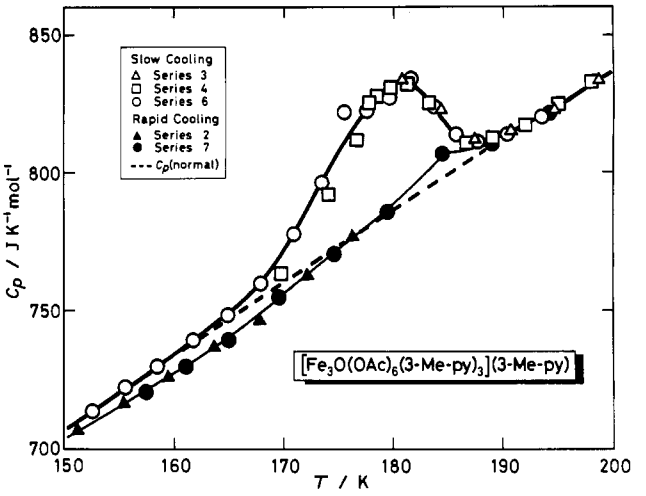

Figure 2. Molar heat capacity of $[Fe_3O(OAc)_6(3\text{-Me-py})_3]\cdot 3\text{-Me-py}$ in the vicinity of the phase transition at 181 K. The broken curve indicates the normal heat capacity.

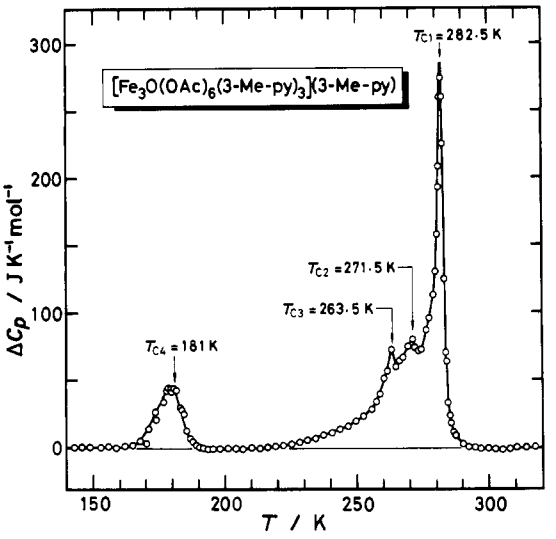

Figure 3. Excess heat capacity, ΔC_p, due to the phase transitions of $[Fe_3O(OAc)_6(3\text{-Me-py})_3]\cdot 3\text{-Me-py}$.

spontaneous stabilization from the undercooled metastable state to the stable state, which occurred partially during the heat capacity measurements. Finally, the measurements in series 8–10 covered the remaining temperature regions for the "slow cooling" specimen.

As a result of the present heat capacity measurements, four phase transitions were found at 181, 263.5, 271.5, and 282.5 K. These transition points will be henceforth designated as T_{C4}, T_{C3}, T_{C2} and T_{C1}, respectively. Since the transition peaks at T_{C2} and T_{C3} are very small, the present DTA measurements failed to detect them. On the other hand, the reason why the anomaly at 181 K did not appear in the DTA thermogram is obviously due to the rapid cooling of the probe employed for the DTA measurements.

In order to determine the enthalpy and entropy associated with these phase transitions, a normal heat capacity curve was estimated by an effective frequency distribution method.[24] The intramolecular vibrational frequencies necessary for this method were assigned on the basis of the observed IR spectra. The curve fitting was made for the slow-cooling specimen by using 61 C_p points in the ranges 12–130 and 300–325 K, in which there seemed to be no effect of any phase transitions. The root-mean-square deviation of the 61 C_p data was ±1.36 J K^{-1} mol^{-1} for the "best" normal heat capacity curve. As shown in Figures 1 and 2 by broken curves, the normal heat capacity curve estimated here

(24) Sorai, M.; Seki, S. *J. Phys. Soc. Jpn.* **1972**, *32*, 382.

Table I. Molar Heat Capacity of the $[Fe_3O(O_2CCH_3)_6(3\text{-Me-py})_3]\cdot 3\text{-Me-py}$ Crystal[a]

T/K	C_p/J K^{-1} mol^{-1}	T/K	C_p/J K^{-1} mol^{-1}	T/K	C_p/J K^{-1} mol^{-1}	T/K	C_p/J K^{-1} mol^{-1}
			Series 1. Slow Cooling[b] to 269 K				
269.136	1080.2	277.757	1135.1	282.600	1277.1	285.413	1082.1
272.028	1096.5	279.871	1175.0	283.981	1125.5	286.858	1073.7
274.905	1103.4	281.249	1241.5				
			Series 2. Slow Cooling to 230 K and Then Rapid Cooling to 12 K				
12.398	35.752	35.680	184.17	69.023	392.08	118.110	619.77
13.518	41.789	37.237	194.50	71.713	408.35	121.056	629.37
14.683	49.409	38.814	205.39	74.443	423.98	124.523	638.73
15.821	56.434	40.409	215.92	77.263	437.69	128.106	646.70
16.918	63.174	42.172	227.67	80.069	452.86	131.801	656.89
18.058	70.160	44.128	240.23	82.899	466.56	135.568	666.54
19.210	76.955	46.112	252.40	85.618	481.33	139.429	676.89
20.392	84.564	48.119	265.36	88.555	496.17	143.316	687.21
21.774	93.416	50.205	278.23	91.557	509.05	147.265	697.30
23.310	102.79	52.301	291.34	94.657	523.28	151.312	707.37
24.851	112.88	54.401	305.00	97.993	538.18	155.414	717.21
26.314	122.32	56.604	318.35	101.348	551.44	159.538	726.30
27.804	132.16	58.915	332.40	104.642	565.14	163.707	737.09
29.416	141.74	61.277	346.73	107.975	578.39	167.923	746.84
31.038	152.64	63.748	361.46	111.294	592.16	172.093	762.75
32.637	163.39	66.350	376.30	114.604	605.90	176.235	776.92
34.172	173.79						
			Series 3. Annealing at 178 K for 18.5 h				
180.893	834.14	187.425	812.21	194.626	823.03	198.685	833.28
184.374	823.26	190.537	814.95				
			Series 4. Slow Cooling to 170 K				
169.925	763.40	192.041	817.30	222.309	897.08	249.835	986.53
174.174	792.37	195.054	824.72	225.327	906.26	252.878	997.81
174.174	792.37	195.054	824.72	225.327	906.26	252.878	997.81
176.799	812.08	198.050	832.58	228.372	915.74	255.902	1011.0
177.836	825.59	201.079	840.51	231.442	924.96	258.902	1030.3
178.867	827.70	204.138	848.27	234.497	934.20	261.904	1054.9
179.897	831.05	207.181	855.64	237.535	944.80	264.916	1065.6
181.437	832.49	210.207	863.96	240.602	953.68	267.909	1080.1
183.490	824.92	213.216	871.45	243.696	964.62	270.878	1100.7
186.573	811.22	216.220	880.29	246.773	974.52	273.833	1100.4
189.068	812.58	219.271	889.09				
			Series 5. Slow Cooling to 257 K				
257.457	1021.3	276.917	1124.5	283.275	1178.1	292.255	1076.8
260.507	1045.7	279.039	1156.1	283.936	1119.0	294.366	1082.1
263.522	1074.9	280.654	1204.9	284.787	1090.3	296.776	1087.0
266.471	1074.4	281.468	1257.0	285.824	1077.8	299.635	1094.7
269.372	1092.8	281.929	1309.9	287.374	1072.8	302.263	1101.0
271.535	1103.5	282.342	1325.3	288.780	1073.4	305.114	1107.7
272.974	1100.8	282.759	1262.5	290.444	1074.3	307.957	1115.2
274.772	1104.0						
			Series 6. Slow Cooling to 99 K				
99.305	539.10	127.395	637.72	152.657	714.25	177.622	822.82
102.340	550.49	130.436	647.81	155.633	723.03	179.641	827.48
105.357	562.25	133.537	658.28	158.687	730.01	181.651	833.90
108.368	573.29	136.602	667.34	161.811	739.75	183.658	824.61
111.430	584.44	139.683	676.67	164.908	748.86	185.671	813.95
114.493	595.79	142.779	686.22	167.978	760.15	187.687	811.30
117.557	606.38	145.845	694.90	171.018	777.45	190.287	813.96
121.389	618.90	148.811	703.79	173.557	796.61	193.463	820.81
124.410	629.12						
			Series 7. Rapid Cooling to 157 K				
157.449	721.00	169.546	755.15	179.463	785.42	189.409	811.45
161.152	729.51	174.533	770.42	184.409	806.67	194.371	821.80
165.020	739.54						
			Series 8. Slow Cooling to 53 K				
53.475	299.11	65.204	368.59	75.949	429.45	87.372	489.02
55.628	312.62	67.769	383.53	78.745	447.28	90.347	501.89
57.880	326.22	70.460	399.27	81.574	461.40	93.375	514.90
60.252	340.27	73.186	413.14	84.449	475.05	96.349	527.94
62.705	354.69						
			Series 9. Slow Cooling to 12 K				
13.057	40.391	19.900	81.444	29.338	141.76	41.250	221.46
14.088	45.899	21.342	90.752	31.155	153.70	43.316	235.47
15.212	52.945	22.931	100.40	33.161	167.15	45.392	247.76
16.339	59.649	24.524	110.57	35.166	181.04	47.461	261.08

Table I (Continued)

T/K	C_p/J K^{-1} mol^{-1}	T/K	C_p/J K^{-1} mol^{-1}	T/K	C_p/J K^{-1} mol^{-1}	T/K	C_p/J K^{-1} mol^{-1}
17.471	66.441	26.118	121.11	37.180	194.28	49.534	273.92
18.644	73.658	27.722	131.61	39.207	208.26	51.596	286.87
			Series 10. Heating to 308 K				
310.746	1124.1	320.999	1152.4	334.126	1194.7	344.713	1217.4
313.930	1132.5	325.002	1164.6	339.237	1207.0	350.159	1229.7
317.446	1141.4	329.380	1178.1				

[a] Relative molecular mass 910.321. [b] "Slow cooling" means a cooling rate of 4 K/h or less, while "rapid cooling" corresponds to a rate of ~2 K/min.

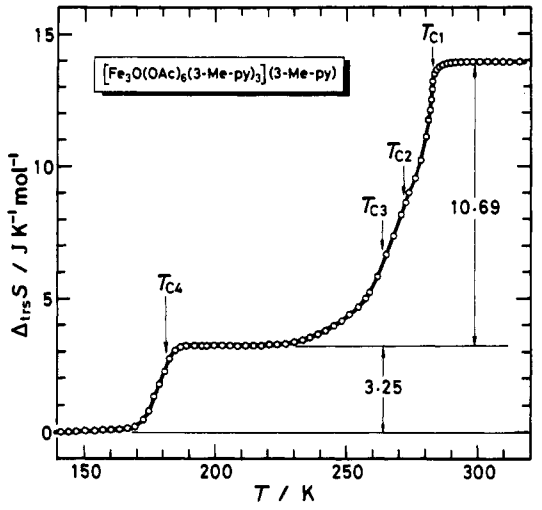

Figure 4. Temperature dependence of the transition entropy of $[Fe_3O(OAc)_6(3\text{-Me-py})_3]\cdot 3\text{-Me-py}$.

seems to have separated rather reasonably the excess contributions due to the phase transitions. Strictly speaking, the normal heat capacity seems to have been somewhat overestimated because it exceeds the observed C_p values by 0.8–1.0 J K^{-1} mol^{-1} in the temperature range from 190 to 215 K. Figure 3 represents the excess heat capacity, ΔC_p, beyond the normal heat capacity curve. The small phase transitions at T_{C2} and T_{C3} are clearly delineated in this figure.

For determination of the transition enthalpy and entropy, the average of the "best three" normal heat capacity curves was employed. The total enthalpy change due to four phase transitions was calculated to be $\Delta_{trs}H$ = 3410 ± 130 J mol^{-1} and the entropy gain $\Delta_{trs}S$ = 13.71 ± 0.65 J K^{-1} mol^{-1}. The temperature dependence of the transition entropy is shown in Figure 4. As revealed by the Mössbauer spectroscopy[11] of $[Fe_3O(O_2CCH_3)_6(3\text{-Me-py})_3]\cdot 3\text{-Me-py}$, this complex gives a Mössbauer spectrum at low temperature (i.e. less than ~60 K) that is comprised of two doublets, one for high-spin Fe^{III} and the other for high-spin Fe^{II}. The Fe^{III}:Fe^{II} spectral area ratio is ~2.0. As the sample temperature is increased, the two doublets are merged into a broad doublet in the range from ~160 to ~220 K, and finally above 296 K the spectrum becomes a sharp quadrupole-split doublet with normal line width. This fact indicates that an "extra" d electron is populated on the unique iron ion in the Fe_3O triad at low temperatures, while at high temperatures the intramolecular electron transfer is occurring rapidly, at least at a rate faster than the ^{57}Fe Mössbauer time scale. Although the variable-temperature Mössbauer spectra do not show any appreciable change at T_{C4} = 181 K and T_{C1} = 282.5 K, it is true that the transition between the electron-localized and -delocalized states is complete, though it occurs over a wide temperature range. If this phenomenon appears as a phase transition(s) in the heat capacity, it contributes R ln 3 to the transition entropy.

Recent X-ray structural work[11] has revealed that the 3-Me-py solvate molecule is disordered in two positions at room temperature. Thus, there is potentially a R ln 2 contribution to the transition entropy associated with the 3-Me-py solvate molecules jumping between the two positions in the solid state. The sum

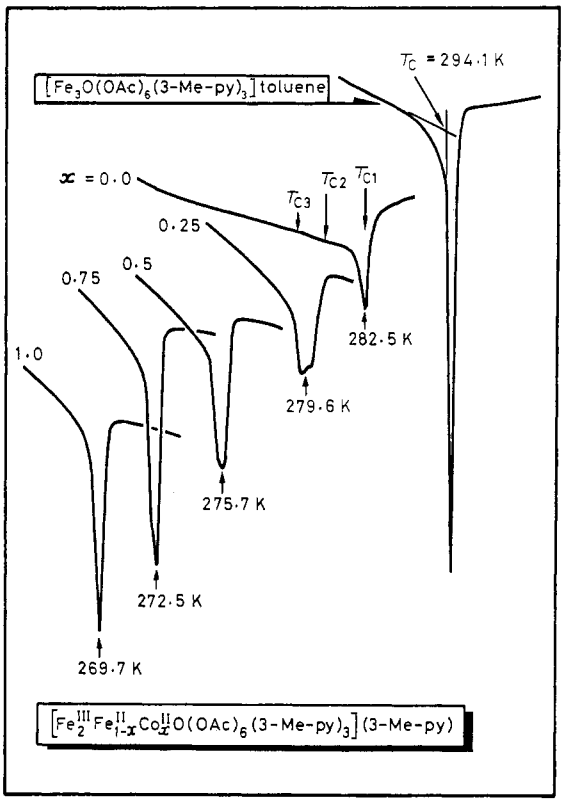

Figure 5. Heating runs of DTA for the solid solutions of $[Fe^{III}_2Fe^{II}_{1-x}Co^{II}_xO(OAc)_6(3\text{-Me-py})_3]\cdot 3\text{-Me-py}$. DTA thermogram for the isostructural $[Fe_3O(OAc)_6(3\text{-Me-py})_3]\cdot$tol is also shown for comparison.

of these two contributions amounts to 14.90 J K^{-1} mol^{-1} (=R ln 3 + R ln 2). This compares favorably with the observed transition entropy of 13.71 ± 0.65 J K^{-1} mol^{-1}. As mentioned above, the present normal heat capacity seems to have been somewhat overestimated and hence the transition entropy has been underestimated. If the normal heat capacity curve is displaced by 0.8–1.0 J K^{-1} mol^{-1} downward over the transition region so that the ΔC_p value in the range from 190 to 215 K will not become negative, the transition entropy is increased to 14.3 ± 0.72 J K^{-1} mol^{-1}. This accounts well the entropy of 14.90 J K^{-1} mol^{-1} arising from the intramolecular electron transfer in the Fe_3O triad and the order–disorder phenomenon of the 3-Me-py solvate molecules.

DTA Thermograms for the Solid Solutions. Now that the observed transition entropy for $[Fe_3O(O_2CCH_3)_6(3\text{-Me-py})_3]\cdot 3\text{-Me-py}$ can be seemingly accounted for in terms of intramolecular electron transfer and the order–disorder phenomenon of the 3-Me-py solvate molecules, the next problem is to elucidate the nature of the particular phase transitions. To this end, DTA measurements were made for the series of solid solutions $[Fe^{III}_2Fe^{II}_{1-x}Co^{II}_xO(OAc)_6(3\text{-Me-py})_3]\cdot 3\text{-Me-py}$ with x = 0.25, 0.50, 0.75, 1.0. Since the intramolecular electron transfer does not occur in $[Fe_2CoO(OAc)_6(3\text{-Me-py})_3]\cdot 3\text{-Me-py}$, the DTA peak(s) relevant to the electron transfer would be diminished with increasing concentration of the Fe_2CoO complex in the Fe_3O matrix. All the DTA thermograms are reproduced in Figure 5,

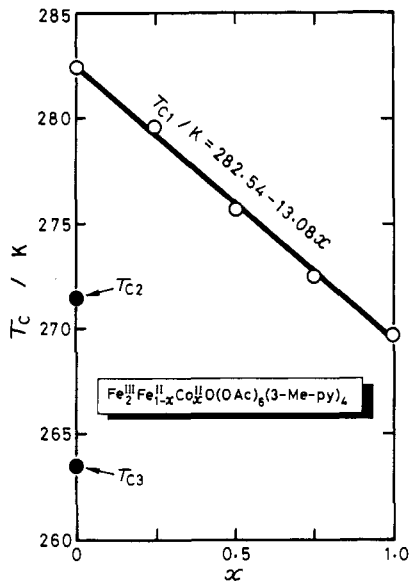

Figure 6. Concentration dependence of the transition point for the solid solutions of $[Fe^{III}_2Fe^{II}_{1-x}Co^{II}_xO(OAc)_6(3\text{-Me-py})_3]\cdot 3\text{-Me-py}$.

where DTA curves for the $x = 0.0$ complex and the isostructural $[Fe_3O(OAc)_6(3\text{-Me-py})_3]\cdot$tol (tol = toluene) are also shown for comparison. The highest temperature phase transition at T_{C1} found for $[Fe_3O(OAc)_6(3\text{-Me-py})_3]\cdot 3\text{-Me-py}$ has a tendency to become sharper with increasing concentration of $[Fe_2CoO(OAc)_6(3\text{-Me-py})_3](3\text{-Me-py})$, x. Furthermore, the peak temperature decreases with increasing x. This situation is illustrated in Figure 6. The concentration dependence of $T_{C1}(x)$ can be described by a linear relationship:

$$T_{C1}(x)\ (\mathrm{K}) = 282.54 - 13.08x$$

This fact indicates that the Fe_3O and Fe_2CoO complexes have been well amalgamated in each solid solution. From the present DTA, it is evident that the phase transition at T_{C1} is mainly associated with the order–disorder phenomenon of the 3-Me-py solvate molecules. A plausible reason the peak found for the Fe_3O complex is broad in comparison with that for the Fe_2CoO complex is that molecular motions of the 3-Me-py solvate molecules might be strongly coupled with the intramolecular electron transfer in the Fe_3O complex, which occurs over a wide temperature region, from ~120 to ~280 K. In contrast, the DTA peak found for the isostructural mixed-valence complex $[Fe_3O(OAc)_6(3\text{-Me-py})_3]\cdot$tol is very sharp. Variable-temperature Mössbauer spectra for this complex[11] show that at the 294.1 K temperature of the phase transition seen in the DTA data the convesion to a single average-valence quadrupole-split doublet is almost completed.

Nature of Phase Transitions. In reference to the phase transition at T_{C4}, the disintegration phenomenon of the 3-Me-py solvate complex at low temperatures observed in the course of X-ray structural analysis[11] should be mentioned here. When a single crystal is cooled below ~100 K, the crystal cracks such that no X-ray structural analysis can be done, and finally, when the same crystal is heated up from ~20 K, it falls into small pieces. The initial cracking phenomenon on cooling seems to be caused by release of the strain energy accumulated in a single crystal during the undercooling process characteristic of the T_{C4} transition. On the other hand, violent disintegration of the crystal on heating would arise from nucleation and growth of the stable crystalline phase in the undercooled metastable matrix.

It is interesting to note here the thermodynamic relationship between the lowest temperature phase and the undercooled phase below T_{C4}. The former phase is transformed into the second lowest temperature phase via the phase transition at T_{C4}, while the latter phase is a simple extension of the second lowest temperature phase. In other words, the higher temperature phase is common to both the phases. It is therefore convenient to compare their molar entropies at a reference temperature, T_{ref}, in this phase. We adopted here 196.8395 K as T_{ref} and estimated the heat capacity of the undercooled phase below 12 K by using the effective frequency-distribution method. The molar entropies at T_{ref}, $S^\circ_{T_{ref}}$, can be obtained by integrating their respective heat capacity curves with respect to ln T in the range from 0 K to T_{ref}. The results are $S^\circ_{T_{ref}}$ (stable lowest temperature phase) = 936.67 J K^{-1} mol^{-1} and $S^\circ_{T_{ref}}$(undercooled phase) = 936.18 J K^{-1} mol^{-1}. They agree well within the present experimental errors of ±1.0 J K^{-1} mol^{-1}. In other words, if we assume that the stable lowest temperature phase obeys the third law of thermodynamics, the undercooled phase also fulfills the third law. Therefore, the undercooled phase belongs not to a thermodynamically nonequilibrium state but to a metastable state. At zero K, different but completely ordered states are established for both phases.

Model for the Phase Transitions. It is now appropriate to try to describe how all of the physical data (X-ray structure, ^{57}Fe Mössbauer spectra, solid-state ^2H NMR spectra on the deuteriated toluene solvate, and heat capacities) can be pieced together to give one model for the phase transition. The model should delineate the microscopic details of how the dynamics of the solvate molecule micromodulate the rate of *intra*molecular electron transfer in the mixed-valence complex.

In Figure 7 is a stereoview of the 298 K solid-state packing arrangement[11] for $[Fe_3O(O_2CCH_3)_6(3\text{-Me-py})_3]\cdot$tol. The 3-Me-py solvate complex is isostructural with this toluene solvate. As can be seen in Figure 7, the Fe_3O complexes in these two compounds are arranged two-dimensionally in layers. The solvate molecule (toluene in one case and 3-Me-py in the other case) is located in a cavity made by three Fe_3O complexes. Thus, if the inherent asymmetry of the 3-Me-py molecule is ignored, the "two-dimensional" packing arrangement of the 3-Me-py solvate (or the toluene solvate) has an approximate threefold symmetry. As indicated above, the solvate molecules in these two compounds are disordered in two lattice positions (see Figure 7). The relatively large thermal parameters associated with these solvate molecules at 298 K suggest that the solvate molecules are dynamically disordered at 298 K. The three 3-Me-py ligands are also each disordered in two positions for both of the compounds. In each layer there are *inter*molecular interactions between Fe_3O complexes, as well as between a given Fe_3O complex and three nearest-neighbor solvate molecules.

Results from the X-ray structural determination[11] of $[Fe_3O(O_2CCH_3)_6(3\text{-Me-py})_3]\cdot 3\text{-Me-py}$ carried out at 128 and 298 K are very suggestive of the nature of the phase transitions observed at 181.4 and ~264–282 K. At 128 K, the Fe_3O triangle is quite distorted with, for example, three different iron–oxide distances: Fe_A–O = 1.936 (2) Å; Fe_B–O = 1.916 (2) Å; Fe_C–O = 1.855 (2) Å. The Fe_3O triangle becomes somewhat more symmetric at 298 K with the following distances: Fe_A–O = 1.925 (5) Å; Fe_B–O = 1.889 (5) Å; Fe_C–O = 1.894 (5) Å. At 298 K the Fe_B–O and

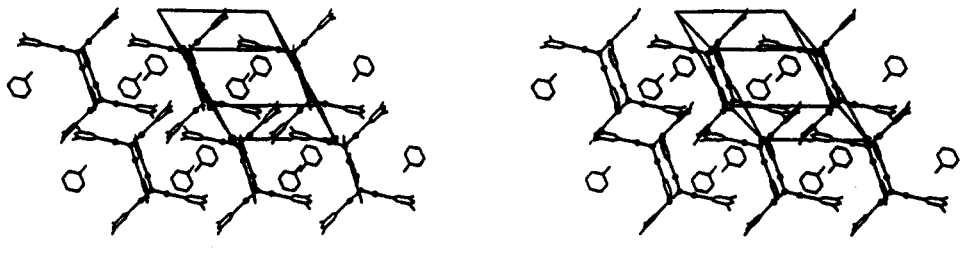

Figure 7. Stereoview of the 298 K solid-state packing arrangement[11] for $[Fe_3O(O_2CCH_3)_6(3\text{-Me-py})_3]\cdot$tol.

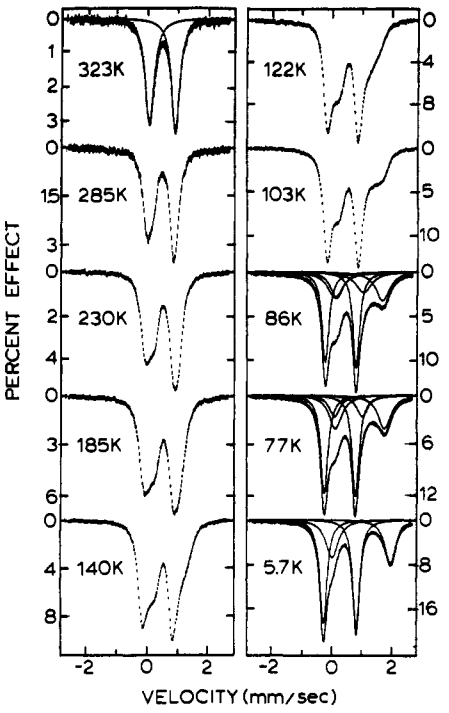

Figure 8. Variable-temperature ^{57}Fe Mössbauer spectra for $[Fe_3O(O_2CCH_3)_6(3\text{-Me-py})_3]\cdot 3\text{-Me-py}$.

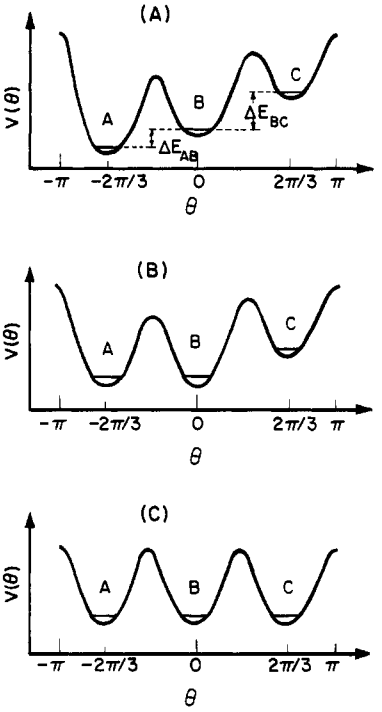

Figure 9. Potential-energy diagrams for an individual Fe_3O complex in the three phases A–C of $[Fe_3O(O_2CCH_3)_6(3\text{-Me-py})_3]\cdot 3\text{-Me-py}$. The potential energy $V(\theta)$ is plotted as a function of direction θ of the molecular distortion with E_g symmetry for the Fe_3O triangle.[18] Only the lowest vibronic level is shown in each potential well.

Fe_C–O distances are essentially comparable.

Variable-temperature ^{57}Fe Mössbauer spectra for $[Fe_3O(O_2CCH_3)_6(3\text{-Me-py})_3]\cdot 3\text{-Me-py}$ are illustrated in Figure 8. From 5.7 to 58 K there are only two doublets in each spectrum, one for high-spin Fe^{III} ions and the other for high-spin Fe^{II} in an area ratio of 2:1 for Fe^{III}:Fe^{II}. In the 77 and 86 K spectra a third "average-valence" doublet is evident, which amounts to ~20% of the spectral area. Above ~103 K it is not possible to fit the spectra to Lorentzian line shapes, for the rate of intramolecular electron transfer is comparable to the inverse of the ^{57}Fe Mössbauer time scale. At the low-temperature (LT) phase transition at 181 K it is clear in Figure 8 that the rate of electron transfer is still increasing with increasing temperature and does *not* exceed the inverse of the ^{57}Fe Mössbauer time scale. It is only by the temperature of the high-temperature (HT) phase transition that a single "average-valence" doublet is seen in the Mössbauer spectrum and the rate of electron transfer is greater than $\sim 10^7$ s^{-1}.

Detailed variable-temperature solid-state ^2H NMR experiments[11] on the isostructural toluene solvate complex indicate the onset of solvate molecule motion occurs in the vicinity of the HT phase transition.

In view of all of the above results, it is likely that below T_{C4} the phase that is present is characterized by distorted Fe_3O complexes with all three iron ions being inequivalent. As illustrated in Figure 9A, the ground-state potential-energy surface for the Fe_3O complexes in this phase would have three minima. The plot in Figure 9A is a simplified, abbreviated view of a "Mexican hat" potential, where each minimum corresponds to one vibronic state with the "extra electron" located on one iron. The ground state in the three potential wells, A–C, shown in Figure 9 corresponds to the electronic–nuclear states of $[Fe_A^{II}Fe_B^{III}Fe_C^{III}]$, $[Fe_A^{III}Fe_B^{II}Fe_C^{III}]$, and $[Fe_A^{III}Fe_B^{III}Fe_C^{II}]$, respectively, where the bond distance between the Fe^{II} ion and the central oxygen atom is longer than those between the Fe^{III} ions and O^{2-} in each state. This molecular distortion arises mainly from the coupling between the 3d electrons and the molecular vibrational mode of the Fe_3O complex. The energy difference, ΔE_{BC}, between the ground states in the potential wells B and C is quite large compared with that (ΔE_{AB}) between the ground states in the potential wells A and B. This comes from the packing arrangement of Fe_3O complexes: since the O–Fe_C–(3-Me-py) moiety is sandwiched tightly by those of the Fe_3O complexes in the layers above and below the relevant layer as seen in Figure 7, the change ($Fe^{III} \rightarrow Fe^{II}$) in the valency of the Fe_C ion associated with an elongation of the O–Fe_C bond requires much energy compared with the cases of the O–Fe_A and O–Fe_B bonds. On the other hand, the packing arrangement around the O–Fe_A–(3-Me-py) moiety is not much different from that around the O–Fe_B–(3-Me-py) moiety. Therefore, the energy difference ΔE_{AB} seems to arise mainly from the cooperative distortion induced by the intermolecular interaction, which results in the difference between the environments around the O–Fe_A and O–Fe_B moieties. A detailed exposition of the electronic structure of these mixed-valence Fe_3O complexes is available.[18] Because of the asymmetry in the solid-state environment, the phase below T_{C4} has one state, i.e., $Fe_A^{II}Fe_B^{III}Fe_C^{III}$, of the three possible states, which is at lowest energy, and it is the only one that is populated at temperatures below T_{C4}.

At T_{C4} it is suggested that the thermal energy has achieved such a value that it is comparable to the energy difference ΔE_{AB}, which is induced by *inter*molecular interactions in the layers of the 3-Me-py solvate complex. When the temperature is increased such that it approaches T_{C4}, the population of the potential well B ($Fe_A^{III}Fe_B^{II}Fe_C^{III}$ state) increases by thermal excitation and the cooperative distortion that stabilizes the state of $Fe_A^{II}Fe_B^{III}Fe_C^{III}$ decreases. The cooperative distortion vanishes sharply at T_{C4}, and as a result the thermally averaged distance of the Fe_A–O bond becomes close to that of the Fe_B–O bond. The Fe_C–O distance does not change noticeably at this phase transition because of strong steric constraint for the O–Fe_C–(3-Me-py) moiety. The ground-state potential-energy surface of an individual Fe_3O complex changes at this point such that above T_{C4} two of the three possible distorted vibronic states, i.e., $Fe_A^{II}Fe_B^{III}Fe_C^{III}$ and $Fe_A^{III}Fe_B^{II}Fe_C^{III}$, have become of more comparable energy (see Figure 9B). Above T_{C4} there is a population in these two vibronic states. If the populations are comparable, ΔS for the T_{C4} phase transition would be $R \ln 2 = 5.76$ J K^{-1} mol^{-1}. This value exceeds the experimental value of $\Delta S = 3.25$ J K^{-1} mol^{-1} for the LT phase transition because it is likely that the two vibronic states are not at exactly equal energies.

The T_{C1} phase transition with its small anomalies (T_{C2} and T_{C3}) is a higher order phase transition as evidenced by its tail (see

Figure 3), which runs down to ~220 K. In the approximate range 250–300 K the solid-state ^2H NMR data show that the solvate molecules of the isostructural toluene solvate start jumping between their two lattice positions. The onset of this motion will soften the lattice about the Fe_3O complexes. As a result the steric constraint for O–Fe_C–(3-Me-py) moieties is weakened and the bond distances of Fe_A–O, Fe_B–O, and Fe_C–O in each Fe_3O complex become more comparable to each other. Then the ground-state potential-energy surface for an individual Fe_3O complex might make a further change as indicated in Figure 9C. The zero-point energies of the three distorted vibronic states would become even more comparable in value. However, from the results of the 298 K structure we know that the three iron ions are not strictly equivalent—there is no crystallographically imposed symmetry for each Fe_3O complex, and the space group remains $A\bar{1}$ from 128 to 298 K. In the limiting case that all three distorted vibronic states are energetically equal as shown in Figure 9C, the contribution to ΔS for the HT (T_{C1}, T_{C2}, and T_{C3}) phase transition from this conversion from two equal states to three would be $\Delta S = R \ln 3 - R \ln 2 = 3.37$ J K^{-1} mol^{-1}. The onset of the 3-Me-py solvate molecules jumping between two positions contributes $\Delta S = R \ln 2 = 5.76$ J K^{-1} mol^{-1}. The total of these two values ($\Delta S = 9.13$ J K^{-1} mol^{-1}) is to be compared with the experimental value of $\Delta S = 10.69$ J K^{-1} mol^{-1} for the HT phase transition. The discrepancy could be accounted for by the fact that the experimental ΔS (=3.25 J K^{-1} mol^{-1}) for T_{C4} fell short of the simple theoretical expectation of $\Delta S = R \ln 2 = 5.76$ J K^{-1} mol^{-1}.

The temperature dependence of the Mössbauer spectra shown in Figure 8 is also explained consistently by the present model. At very low temperature, only the state of $Fe_A^{II}Fe_B^{III}Fe_C^{III}$, which corresponds to the potential well A in Figure 9A, is occupied. Only two doublets, one for the two Fe^{III} ions and the other for the one Fe^{II} ion, are expected in the Mössbauer spectra. When the temperature increases, the population of the state $Fe_A^{III}Fe_B^{II}Fe_C^{III}$ in the potential well B increases and small domains of minority phase (high-temperature phase) are created and continue to grow. The Fe_3O complexes in the minority phase have the potential energy surface shown in Figure 9B, where the extra electron is delocalized between the Fe_A and Fe_B ions by tunneling. The third doublet in the 77 and 86 K Mössbauer spectra comes from the Fe_A and Fe_B ions in the minority domains, while the first and second doublets come from the Fe_C ions in the minority domains and the Fe_A, Fe_B, and Fe_C ions in the majority domains in which the Fe_3O complexes have the potential-energy surface shown in Figure 9A. After the phase transition at T_{C4}, the Fe_3O complexes with the potential surface of Figure 9B are in the majority. When the temperature increases above T_{C4}, the 3-Me-py solvate molecules start jumping between their two lattice positions. This stabilizes the state of the Fe_3O complex corresponding to the potential-energy surface shown in Figure 9C, in which the extra electron is transferring rapidly between the three Fe ions, Fe_A, Fe_B, and Fe_C. The Mössbauer spectrum arising from this completely "delocalized" state consists of only one doublet. The Mössbauer spectra for temperatures between T_{C4} and T_{C1} arise from a superposition of spectra of the completely "delocalized" state with spectra of the partially delocalized state, which comes from the potential surface of Figure 9B. The mixing ratio increases with increasing temperature. After the phase transition at T_{C1} the Fe_3O complexes in the completely "delocalized" state are in the majority. Then, the Mössbauer spectrum consists of one doublet as shown in Figure 8.

All in all, the present model for the three different phases of $[Fe_3O(O_2CCH_3)_6(3\text{-Me-py})_3]\cdot 3\text{-Me-py}$ does explain reasonably well all of the physical data for this complex.

Summary and Comments

Basically two phase transitions have been found in the C_p data taken in the range 12–350 K for mixed-valence $[Fe_3O(O_2CCH_3)_6(3\text{-Me-py})_3]\cdot 3\text{-Me-py}$. The LT phase transition at ~181 K is easily undercooled. The HT phase transition is a higher order phase transition starting at ~220 K and culminating at 282.5 K with two anomalies at 263.5 and 271.5 K. ΔS for the LT phase transition was found to be 3.25 J K^{-1} mol^{-1}, whereas the HT phase transition has $\Delta S = 10.69$ J K^{-1} mol^{-1}.

A model that fits all available C_p, X-ray crystallographic, and spectroscopic data has been devised. The LT phase transition is suggested to involve a change in the solid such that above ~181 K the "extra" electron in a Fe_3O complex is transferring relatively rapidly between two of the three iron ions. The HT phase transition clearly involves the onset of solvate molecule dynamics wherein each 3-Me-py solvate molecule jumps between two lattice positions. This onset of solvate molecule motion in essence serves as a micromodulation of the environment about each Fe_3O complex. When the three vibronic minima of the potential-energy surface become more comparable in energy as a result of the dynamics of the solvate molecules symmetrizing the environment about a given Fe_3O complex, the rate of intramolecular electron transfer between all three iron ions increases dramatically. This increase in the rate probably largely reflects an increase in the rate of quantum-mechanical tunneling due to more comparable energy of the vibronic states.

Additional direct evidence about the microscopic nature of the LT phase transition at ~181 K is needed. It would be interesting to have the X-ray structure at 200 K. Also, solid-state ^2H NMR spectroscopy should be used to study a deuteriated acetate form of the 3-Me-py solvate complex. The CD_3 groups of the acetate groups would serve as monitors of changes in electronic localization in the Fe_3O complex in and around the LT and HT phase transitions. This approach served well in studying $[Fe_3O(O_2CCD_3)_6(py)_3]\cdot py$.[10]

Acknowledgment. M.S. wishes to express his sincere thanks to the Ministry of Education, Science and Culture for a Grant-in-Aid for Scientific Research. D.N.H. is grateful for funding from the National Institutes of Health, Grant HL13652.

Registry No. $[Fe_3O(O_2CCH_3)_6(3\text{-Me-py})_3]\cdot 3\text{-Me-py}$, 105943-92-8; $[Fe_2CoO(O_2CCH_3)_6(3\text{-Me-py})_3]\cdot 3\text{-Me-py}$, 105969-25-3; Fe, 7439-89-6.